Results in Physics 55 (2023) 107189

Contents lists available at ScienceDirect

Results in Physics

journal homepage: www.elsevier.com/locate/rinp

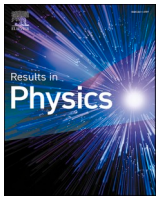

Mixed compensation for the testing of large convex aspheres

Xiaokun Wang [a,b,c,d], Zhongkai Liu [a,b,c,d], Hang Su [a,b,c,d,*], Qiang Cheng [a,b,c,d], Lingzhong Li [a,b,c,d], Fukun Li [a,b,c,d], Wenyan Li [a,c,d], Bin Liu [a,b,c,d], Jing Wang [a,b,c,d], Mengxue Cai [a,b,c,d], Jincheng Wang [a,c,d], Wenhan Li [a,b,c,d], Luojia Zhang [a,b,c,d], Qiong Wu [a,b,c,d], Xiao Luo [a,b,c,d], Xuejun Zhang [a,b,c,d]

[a] Changchun Institute of Optics, Fine Mechanics and Physics, Chinese Academy of Sciences, Changchun, Jilin 130033, China
[b] University of Chinese Academy of Sciences, Beijing 100049, China
[c] Key Laboratory of Optical System Advanced Manufacturing Technology, Changchun, Jilin 130033, China
[d] State Key Laboratory of Applied Optics, Changchun, Jilin 130033,China

ARTICLE INFO

Keywords:
Optical testing
Large convex asphere
Mixed compensation
Sub-aperture stitching testing
CGH

ABSTRACT

Since the testing of convex mirrors often requires a compensator with a larger aperture than the mirror under test, this is undoubtedly a trade-off not worth pursuing. Moreover, for surfaces with higher levels of asphericity, it further escalates the challenges in testing. In this study, high-accuracy testing of large convex aspheric surfaces with rotary symmetry was achieved via a method that combines sub-aperture stitching and Computer-Generated Holograms (CGH) compensation testing. Applying the methodology outlined in this study, practical testing was conducted on a large-aperture convex aspheric mirror with a diameter of 538 mm. The outcomes demonstrated that the center testing data and the outer ring testing data were stitched by the stitching algorithm to obtain the surface error of the full-aperture. The results were compared to those of Luphoscan and compensation testing, with a residual Root Mean Square (RMS) less than $\lambda/20$ ($\lambda = 632.8$ nm). Finally, the error analysis of the entire testing process showed that the accuracy was better than $\lambda/50$. The results demonstrate that the method can achieve highly accurate test of large convex aspheric surfaces.

Introduction

With the rapid development in fields such as astronomical optics [1–7] and applied optics [8–10], achieving higher resolutions in optical systems has led to an increasing trend in aperture sizes. Consequently, this has placed elevated demands on optical manufacturing and testing techniques. In optical systems, aspherical optical elements have more design freedom, and can therefore satisfy more complex design requirements. In addition, the introduction of aspherical elements can improve image quality by increasing the field of view and resolution. Furthermore, the use of aspheric surfaces can reduce the number of elements, thus reducing the complexity of the system for the same performance specifications. Therefore, aspherical mirrors are increasingly used in space optics, astronomical optics, military technology, and high-tech civil applications. In the field of astronomical observation, the resolution of the optical imaging system has more strict requirements. Therefore, the aperture of the optical elements has also increased [11–14]. For example, China Space Station Telescope (CSST) will launch in 2025 features a secondary mirror with a diameter of 450 mm, which is a large convex aspheres mirror. The secondary mirror of the recently launched James Webb Space Telescope (JWST) has a convex aspherical surface and an aperture of 738 mm. Corresponding testing technology has also been developed to meet these requirements [15,16].

Traditional methods for testing aspherical convex surfaces include profile measurement, aberration-free point measurement, compensation measurement, and sub-aperture stitching. Profile measurement has limitations in aperture size, extended testing time, and restricted precision. The method of aberration-free point testing is only suitable for the testing of specific quadratic surfaces [17–22]. When testing large-aperture convex aspheres, a larger Hindle sphere mirror often needs to be used, which can introduce center obscuration issues during the measurement process. Employing compensation elements alone for full-aperture surface form testing requires the fabrication of aspherical compensating lenses with larger apertures matching the test mirror, or CGH with high spatial frequency for significant departure from flatness in large aperture aspheres. However, when applied to large aperture

* Corresponding author at: Changchun Institute of Optics, Fine Mechanics and Physics, Chinese Academy of Sciences, Changchun, Jilin 130033, China.
E-mail address: suhang971223@163.com (H. Su).

https://doi.org/10.1016/j.rinp.2023.107189
Received 31 August 2023; Received in revised form 8 November 2023; Accepted 13 November 2023
Available online 19 November 2023

convex aspheres, using stitching alone results in a substantial number of sub-aperture, increasing testing time and complicating data processing. Furthermore, this exacerbates error accumulation, thus limiting the accuracy of stitching testing. When using the CGH to test large aperture aspheres with significant departure from flatness, it requires CGH with high spatial frequency, which poses challenges in terms of manufacturing complexity, cost, and the difficulty of alignment and calibration. Consequently, employing the CGH-based testing approach alone becomes impractical for inspecting large aperture convex aspheres with substantial departure from flatness [22–25]. Professor W. Osten from the University of Stuttgart in Germany proposed the Tilted-Wavefront-Interferometry based on the non-null interferometric principle in 2007 [26]. In this interferometric setup, a lens array is used in the interference optical path to introduce multiple off-axis testing beams. These beams generate spherical waves with different tilt angles to compensate gradients in various local regions on the test surface error, enabling measurements of aspherical and freeform surfaces. Compared to fully compensated measurement techniques, this method does not require customized and expensive CGH compensators, making it more versatile. It has been successfully applied to small-diameter freeform surface measurements, achieving a precision of λ/30 (RMS) [26–32]. This achievement is exceptional. The method offers a wide dynamic range and can complement the limitations of CGH in measuring steep freeform surfaces. Moreover, it holds promising potential for large-diameter freeform surface measurements.

In this study, the approach of combining CGH with sub-aperture stitching testing can reduce the fabrication aperture of compensating elements and also minimize the number of Sub-aperture, thereby reducing stitching errors. Finally, to obtain the surface error of the full-aperture, the testing data of the center and outer rings were stitched together using the sub-aperture stitching algorithm. This method expands the measured aperture range via the CGH compensation method, thus increasing the planned sub-aperture size and achieving the aim of reducing the number of sub-aperture. Therefore, this method not only reduces the transmission of errors and improves the testing efficiency, but it also reduces testing costs [33–39].

Theory and method

Principle of central sub-aperture testing

Because the central asphericity of the large convex mirror is small, the method of Non-null testing can be used, so the interferometer can be used for direct measurement. The plane wavefront out of the interferometer was converted into a spherical wave through the standard lens, and the light was incident on the testing surface along the normal direction and it returned approximately along the original path. During the measurement process of the central sub-aperture, it is advisable to choose an appropriate standard lens and directly measure it using an interferometer. When selecting the standard lens, the following principles are applied for its selection:

$$F^{\#} = \frac{f}{D} \tag{1}$$

where F# is the F number of the standard lens, f is the standard lens focal length, D is the standard lens aperture.

$$R^{\#} = \frac{R}{d} \tag{2}$$

R# is the R number of the central sub-aperture, R is the best fitting spherical radius of the central sub-aperture apex, and d is the central sub-aperture size. The selection criterion is $F^{\#} \le R^{\#}$ and $f > R$. The R number is calculated using Formula (2), and based on this calculation, the most suitable standard lens is selected.

The size of the central aperture is determined based on the spot size. When measuring the central sub-aperture, the incident light was not incident along the direction normal to the testing aspheric surface because it was a standard spherical lens that directly tested the aspheric surface, which introduced a corresponding non-common path error. This part of the error was caused by the deviation between the aspheric surface and the best fitting spherical surface, which was obtained by subtracting the two normal from each other and was removed in the stitching algorithm.

The parameters of the mirror to be tested were as follows: diameter D = 538 mm, vertex radius of curvature r = 1371.905 mm, and quadratic curve constant k = -1.588687. The size of the central sub-aperture was 124.7 mm, and the size of the outer circle aperture was 245 mm. The distance between the center of the outer circle aperture and the center of the mirror to be examined was 168 mm.

The radii of curvature and asphericity of the center and outer circular apertures were calculated separately according to the plan. The center sub-aperture's the best fitting spherical radius of curvature was 1373 mm and its asphericity was 193.7219 nm, and the outer circle aperture's the best fitting spherical radius of curvature was 1403 mm and its asphericity was 6.6212×10^4 nm. According to the calculation results, the asphericity of the center sub-aperture was small and could be tested directly without compensation. The asphericity of the outer circle aperture was larger, and its interference fringe density was also larger; thus, the latter exceeded the limit of the resolution of the interferometer's CCD camera. Hence, the fringe density needed to be reduced via the compensation method in order to proceed with the testing.

Outer sub-aperture layout method and compensation testing model using CGH

Because the deviation at edge of aspheric surface was large, the method of Null-Compensation testing was used, and the CGH compensation element was used to convert the spherical wavefront into aspherical wavefront which fit the theoretical aspherical mirror. The light was incident along the normal and returned in the original way, forming interference fringes with the reference wavefront. It is necessary to ensure that the planned sub-aperture size can achieve coverage of the full-aperture and that the overlapping area of each adjacent sub-aperture is generally larger than 25 % of the sub-aperture area.

The size of the outer circular aperture depended on the CGH testing design. Based on the size of the testing-area of the CGH and the distance between it and the examined mirror, the size of the spot on the examined mirror was obtained via light tracing to determine the outer circle aperture. The number of outer circle apertures was determined according to the principle of sub-aperture planning.

A CGH is generally divided into three zones: a main zone (which is the testing zone) used to test the surface error of the examined mirror, an alignment zone used to align the interferometer and the CGH, and a reference zone used to align the CGH and the examined mirror. When designing the main area, the test optical path should return along the original path until the differences between the wave images are minimized, and the diffraction pattern fringe density should satisfy the existing CGH processing production conditions.

The optical path of the main area of the CGH is shown in Fig. 1. The CGH surface near the mirror to be examined was designed to approach the Zernike Fringe Phase. The main diffraction level of the main area was set to + 1, and the left focus/point source is not on the axis of the collimating lens, but laterally shifted in y-direction by 5 mm. Then, there is a tilt angle of the plane wave between lens and CGH of about 5 mm/focal length of the lens which avoids that the directly reflected light at the CGH substrate enters the interferometer.

The first three items of the Zernike Polynomial front 37 items were set to 0, and the other items were set to variable for the CGH diffraction pattern was optimized so that the reflected light returned along the original path and the value of the wavefront aberration reached a minimum. The Zernike coefficient was the design parameter of the CGH

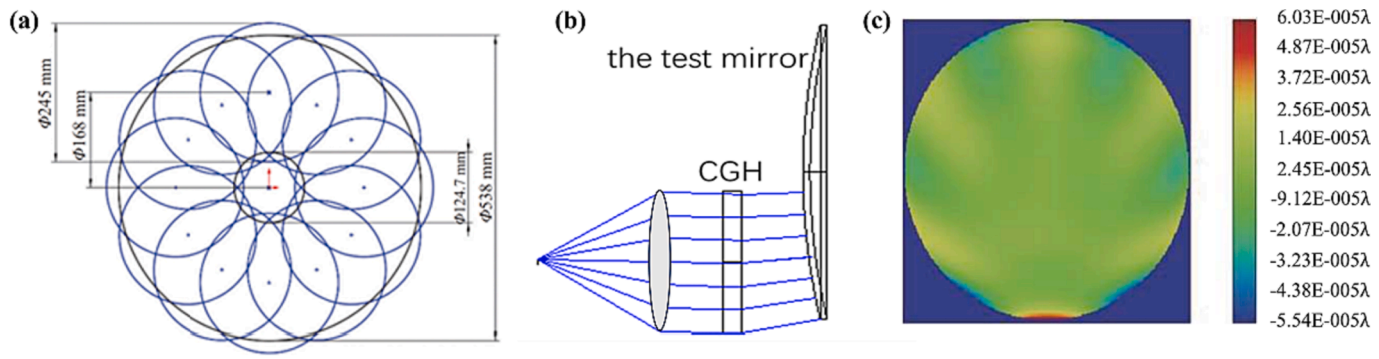

Fig. 1. The panning of sub-aperture (a) Sub-aperture planning. (b) The optical path of the testing-area of the CGH design. (c)Testing wavefront of the testing-area of the CGH.

during this experiment. Fig. 1(b) represents the optical design of the interferometer combined with CGH for testing. It is noteworthy that load a tilt in the CGH can result in off-axis aberrations. However, compensations have been applied during the design of the CGH (testing mirror and the CGH can be compensated each other). Fig. 1(c) illustrates the design residual errors, with Peak to Valley (PV) $= 1.157 \times 10^{-4}\lambda$ and RMS $< 0.0001\lambda$, indicating that the design residuals are very small and can thus be ignored. Here, $\lambda = 632.8$ nm.

Stitching algorithm and theoretical derivation

Because the central asphericity of the large convex mirror is small, the method of Non-null testing can be used, so the interferometer can be used for direct measurement. The plane wavefront generated by the interferometer is transformed into a spherical wavefront through a standard lens. The light is incident to the testing surface along the normal direction of the best fitting sphere and is subsequently received by the interferometer. Consequently, non-common path errors exist. out-of-focus aberrations. First, the central sub-aperture is selected as the reference sub-aperture. The adjustment coefficients for other sub-aperture relative to the central reference sub-aperture are denoted as (a_1, b_1, c_1, p_1), (a_2, b_2, c_2, p_2), (a_3, b_3, c_3, p_3), …, $(a_{M-1}, b_{M-1}, c_{M-1}, p_{M-1})$. Assuming the phase distribution for the reference sub-aperture is w_o, the relationship of the phase distribution for other Sub-aperture with respect to the reference sub-aperture can be expressed as:

$$w_0 = w_1 + p_1 + a_1x_1 + b_1y_1 + c_1(x_1^2 + y_1^2) = w_2 + p_2 + a_2x_2 + b_2y_2 + c_2(x_2^2 + y_2^2)\cdots = w_{M-1} + p_{M-1} + a_{M-1}x_{M-1} + b_{M-1}y_{M-1} + c_{M-1}(x_{M-1}^2 + y_{M-1}^2) \quad (3)$$

In the equation, w_1, w_2, …, w_{M-1}represent the phase data of other sub-aperture, where M is the number of sub-aperture. a_1, a_2,…, $a_{M-1}$and b_1, b_2,…, b_{M-1} are the tilt coefficients along the x and y directions, respectively, for other sub-aperture relative to the reference sub-aperture. c_1, c_2,…, c_{M-1} and p_1, p_2,…, $p_{M-1}$are the defocus and shift coefficients, respectively.

Through least squares fitting, the sum of squares of phase differences in all overlapping regions is minimized, as shown in Equation (4):

$$S = \sum_{j_1\neq 0}^{N_1}\sum_{i_1\subset W_0, W_{j_1}}^{n_{ij}}\{W_0(x_{0i_1}, y_{0i_1}) - [W_{j_1}(x_{j_1i_1}, y_{j_1i_1}) + p_{j_1} + a_{j_1}x_{j_1i_1} + b_{j_1}y_{j_1i_1} + c_{j1}(x_{j_1i_1}^2 + y_{j_1i_1}^2)]\}^2 + \sum_{j_2\cap j_3\neq 0}^{N_2}\sum_{i_2\subset W_{j_2}, W_{j_3}}^{n_{ij}}\left\{\left[W_{j_2}(x_{j_2i_2}, y_{j_2i_2}) + p_{j_2} + a_{j_2}x_{j_2i_2} + b_{j_2}y_{j_2i_2} + c_{j_2}(x_{j_2i_2}^2 + y_{j_2i_2}^2)\right] - \left[W_{j_3}(x_{j_3i_2}, y_{j_3i_2}) + p_{j_3} + a_{j_3}x_{j_3i_2} + b_{j_3}y_{j_3i_2} + c_{j_3}(x_{j_3i_2}^2 + y_{j_3i_2}^2)\right]\right\}^2 = \min \quad (4)$$

Detailed error analysis will be conducted in the subsequent sections. Due to the deviation at the edge of aspheric surface was large, the method of Null-Compensation testing was used, and the CGH compensation element was used to convert the spherical wavefront into aspherical wavefront which fit the theoretical aspherical-Mirror. The light was incident along the normal and returned in the original way, forming interference fringes with the reference wavefront. Finally, using a sub-aperture stitching algorithm to calculate the full-aperture error distribution of the large convex aspherical surface.

In the process of stitching the outer circle apertures, there was a certain overlap between the sub-aperture, and the phase data were used to minimize the relative error between adjacent sub-aperture. Because the outer circle apertures were tested in a null-position, the relative misalignment between the sub-aperture could cause translation, tilt, and

There are two types of overlapping regions: one where other sub-aperture overlap with the central reference sub-aperture, defined as j_1, with values ranging from 1 to N_1. The other type involves overlapping regions between Sub-aperture other than the central reference sub-aperture. Two Sub-aperture involved in such overlaps are denoted as j_2 and j_3, with values ranging from 1 to N_2.$(x_{j_1i_1}, y_{j_1i_1})$ represents the coordinates of sampling points in the overlap region i_1 between sub-aperture j_1 and the reference sub-aperture W_0. Similarly, j_2 and j_3 represent two adjacent sub -aperture. $(x_{j_2i_2}, y_{j_2i_2})$ represents the coordinates of sampling points in overlap region i_1 between sub-aperture j_2 and sub-aperture j_3 within sub-aperture j_2. $(x_{j_3i_3}, y_{j_3i_3})$ represents the coordinates of sampling points in overlap region i_2 between sub-aperture j_2 and sub-aperture j_3 within sub-aperture j_3. n_{ij} represents the number of sampling points in each overlapping region.

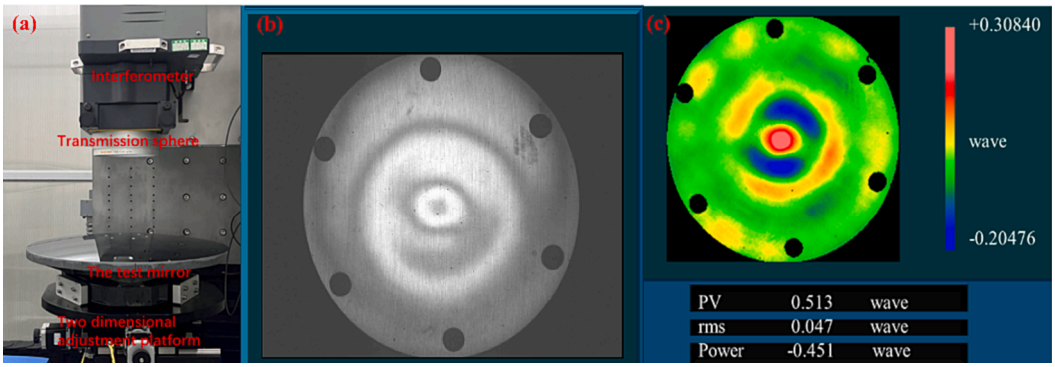

Fig. 2. (a) The optical path used in the central sub-aperture tests. (b) the interference fringes of central sub-aperture. (c) The surface error of center sub-aperture.

Taking partial derivatives of each stitching factor, setting them to zero leads to Equation (5):

$$\begin{cases} \dfrac{\partial S}{\partial p_i} = 0 \\ \dfrac{\partial S}{\partial a_i} = 0 \\ \dfrac{\partial S}{\partial b_i} = 0 \\ \dfrac{\partial S}{\partial c_i} = 0 \end{cases} \tag{5}$$

For $1 \le i \le M-1$, analyzing and solving Equation (4) leads to the final least squares equation given in Equation (6):

$$\sum_{i=0}^{M-1}\sum_{j=1}^{M-1} P_{ij} = \sum_{i=0}^{M-1}\sum_{j=1}^{M-1}\left[(Q_{ij} - \delta_{ij}\cdot Q_{ij})\cdot R_{ij}\right] \tag{6}$$

The expressions for matrices P, Q, and R are as follows:

$$P_{ij} = \begin{bmatrix} \sum_{i\cap j} x\Delta w \\ \sum_{i\cap j} y\Delta w \\ \sum_{i\cap j}(x^2+y^2)\Delta w \\ \sum_{i\cap j}\Delta w \end{bmatrix} \tag{7}$$

$$Q_{ij} = \begin{bmatrix} \sum_{i\cap j} xx & \sum_{i\cap j} xy & \sum_{i\cap j} x(x^2+y^2) & \sum_{i\cap j} x \\ \sum_{i\cap j} yx & \sum_{i\cap j} yy & \sum_{i\cap j} y(x^2+y^2) & \sum_{i\cap j} y \\ \sum_{i\cap j}(x^2+y^2)x & \sum_{i\cap j}(x^2+y^2)y & \sum_{i\cap j}(x^2+y^2)^2 & \sum_{i\cap j}(x^2+y^2) \\ \sum_{i\cap j} x & \sum_{i\cap j} y & \sum_{i\cap j}(x^2+y^2) & \sum_{i\cap j} n_{ij} \end{bmatrix} \tag{8}$$

$$Q_{ii} = \begin{bmatrix} 0 & 0 & 0 & 0 \\ 0 & 0 & 0 & 0 \\ 0 & 0 & 0 & 0 \\ 0 & 0 & 0 & 0 \end{bmatrix} \tag{9}$$

$$R_{ij} = \begin{bmatrix} a_{ij} \\ b_{ij} \\ c_{ij} \\ p_{ij} \end{bmatrix} \tag{10}$$

$$\delta_{ij} = \begin{cases} 1 & i \leqslant j \\ 0 & i > j \end{cases} \tag{11}$$

In the equation, if there is no overlap between any two sub-apertures, the sub-matrices P_{ij} and Q_{ij} are zero matrices. Where n is the number of sampling points in each overlapping region; i is an integer ranging from 0 to M−1; j is an integer ranging from 1 to M−1. This globally optimized stitching algorithm significantly reduces stitching errors, accomplishes the merging of all sub-aperture, and thereby yields the complete surface profile data.

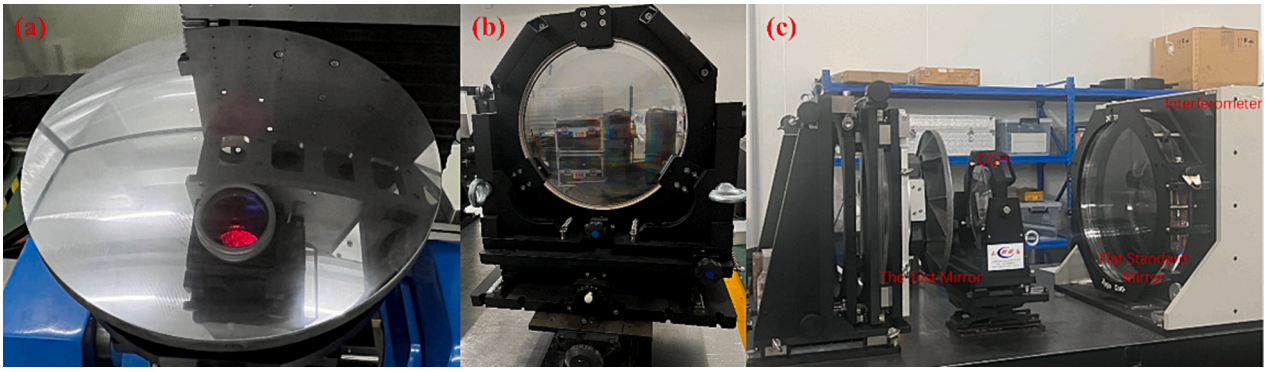

Fig. 3. (a) The testing mirror. (b) Physical diagram of the CGH. (c)The testing optical path of the outer sub-aperture.

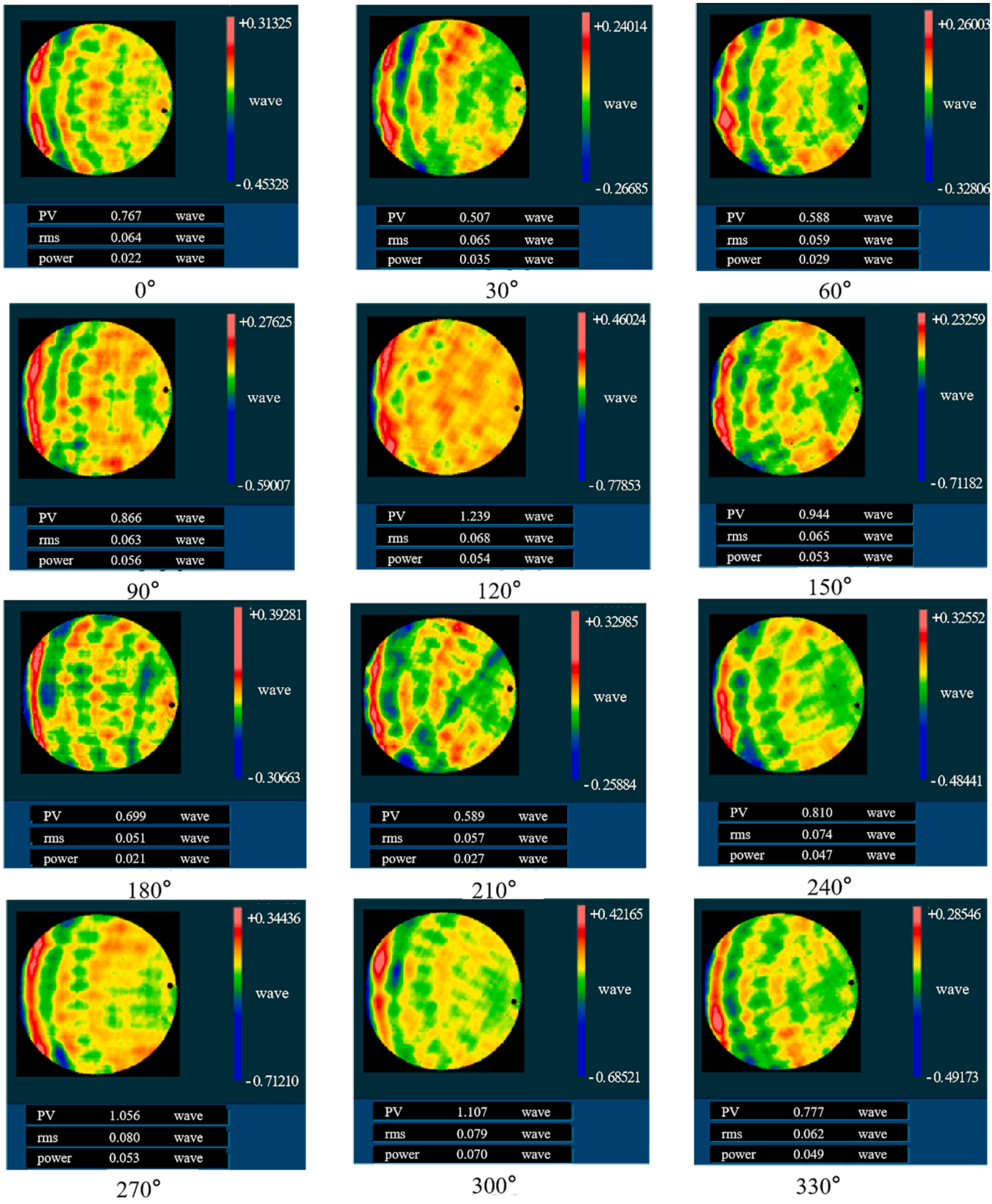

Fig. 4. The surface error of outer Sub-aperture.

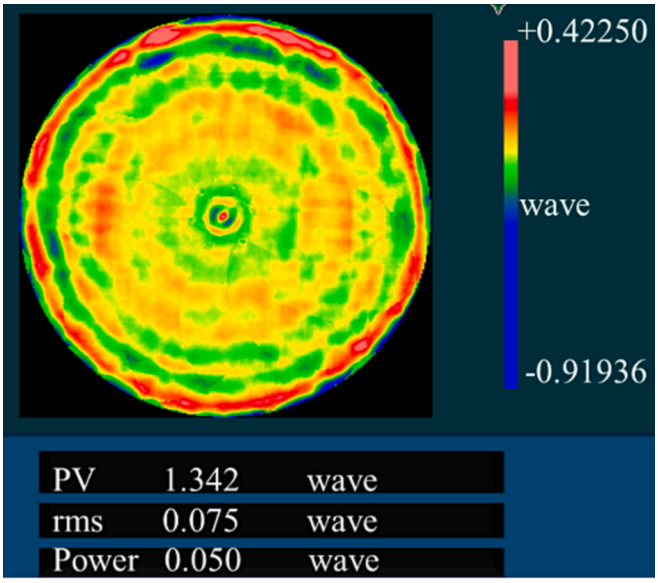

Fig. 5. The result of sub-aperture stitching.

Experimental

To demonstrate the feasibility of the testing method that combined CGH compensation and stitching, experiments were designed. This section describes specific examples of these experiments. Testing experiments and stitching results.

Center sub-aperture testing

According to the interferometer's center aperture testing schematic used to construct the optical path, the F#11 standard lens was installed. The interferometer's positions were aligned so that the reflected light approximately followed the original path. The testing optical path is illustrated in Fig. 2 (a), The central sub-aperture of the large convex aspheric surface was tested by adjusting the distance between the standard lens and the mirror to be examined. To minimize the interference fringes, the focal point of the standard lens and the center of the examined mirror closest to the spherical center of the ball coincided. The non-common error was obtained by subtracting the aspheric surface of the central sub-aperture from its nearest spherical normal. Then, to obtain the surface error of the face of the central sub-aperture, the non-common error was subtracted from the result obtained via interferometer testing. As shown in Fig. 2. (c)the final surface errors obtained using the centroid aperture were 0.513λ (PV) and 0.047λ (RMS).

Outer sub-aperture testing

Because of the outer ring's large asphericity, the CGH compensation method was required to test it. The test optical path is shown in Fig. 3.

First, the reference area of the CGH was aligned with the interferometer, and then the mirror to be tested was adjusted by changing the translation, pitch, and twist values on the x, y, and z-axes of the frame.

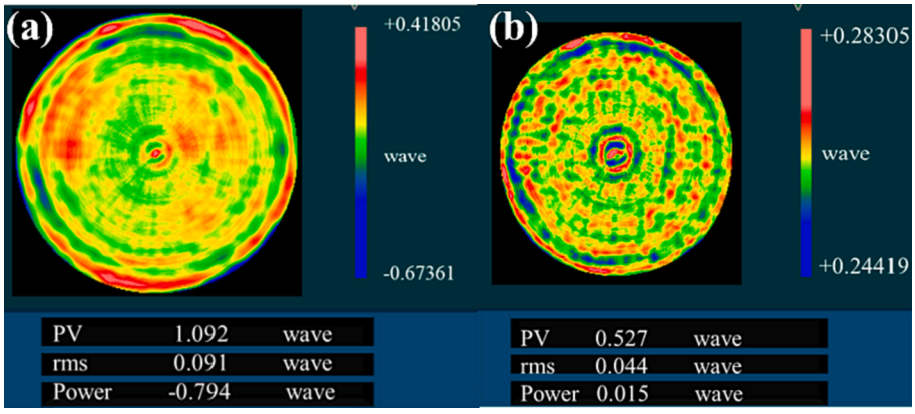

Fig. 6. (a)The testing result of the Luphoscan. (b)The residuals between the stitching result and Luphoscan test result.

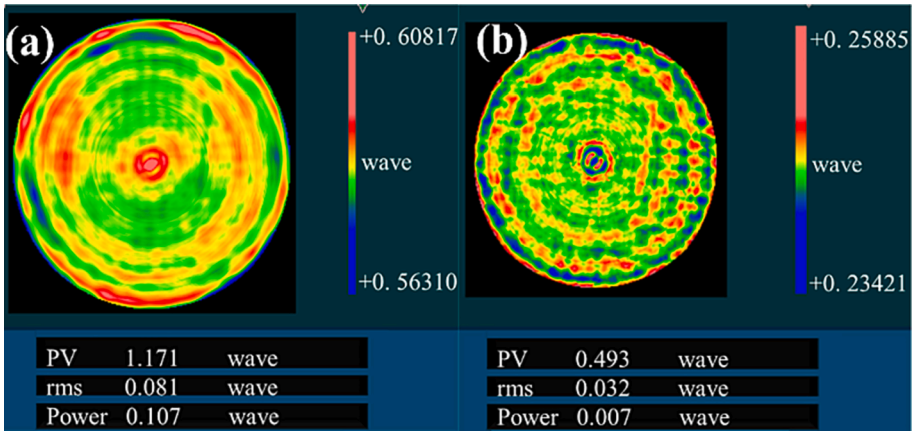

Fig. 7. (a)The results of the compensation mirror's testing of the surface error of the full-aperture. (b) The residuals between the stitching results and the compensating mirror's testing results.

Table 1
CGH error analysis.

The error of CGH	Value
Design error	$<1 \times 10^{-4}\lambda$
Coding error	$7.02 \times 10^{-4}\lambda$
Characterization distortion	$1.24 \times 10^{-4}\lambda$
Duty cycle error	$5.75 \times 10^{-3}\lambda$
Refractive index inhomogeneity	$6.87 \times 10^{-5}\lambda$
RSS	$5.79 \times 10^{-3}\lambda$(3.67 nm)

The alignment area of the CGH was used to adjust the bit attitude between the CGH and the mirror to be tested until the testing fringe was zero. The results of the outer circle aperture tests are shown in Fig. 4.

Full-Aperture stitching

Based on the principles of the stitching algorithm outlined in the second section, develop a corresponding stitching algorithm. Utilize this stitching algorithm to seamlessly integrate the testing results of the outer sub-aperture and the inner sub-aperture. Fig. 5 shows the surface error of the full-aperture obtained using the stitching algorithm, with the value were 1.342λ (PV) and 0.075λ (RMS).

Comparative experiments and comparative results

To verify the correctness of the CGH-based stitching compensation method used for testing large convex aspheric surfaces, two different full-aperture testing methods were designed, and the results obtained from stitching were compared to those obtained from full-aperture testing.

Profilometer Luphoscan testing experiment

Fig. 6(a) shows the results for the surface error of the full-aperture, with the value were 1.092λ (PV)and 0.091λ(RMS). Fig. 6(b) shows the residuals between the stitched and Luphoscan results, were 0.527λ (PV) and 0.044λ (RMS), which were obtained via point-to-point subtraction of the tested results from the stitched surface error of the full-aperture.

Compensator testing experiment

Fig. 7(a) shows the results were1.171λ (PV) and 0.081λ (RMS). Fig. 7 (b)shows the residuals between the stitch results and the Null-compensation testing results, with the result were 0.493λ (PV) and 0.032λ (RMS), which were obtained after point-to-point subtraction from the results of the stitch surface error of the full-aperture.

After point-to-point subtraction of the test results of the two comparison experiments from the stitching test results, the residual RMS was less than λ/20. The feasibility of the Mixed-Compensation for testing large convex aspherical mirrors was verified by comparing the sub-aperture stitching and CGH hybrid compensation testing results of large convex aspherical mirrors to those of full-aperture testing experiments.

Error analysis

System error

In the process of producing amplitude-CGH, certain errors occurred before the fabrication processes were complete. These included CGH design error, coding error, etching distortion, duty cycle errors. Table 1 shows the CGH error results, with the fabrication error of $5.79 \times 10^{-3}\lambda$ and the theoretical accuracy of 3.67 nm.

In this study, the accuracy of the stitching experiment was evaluated using a self-test. The self-test involved designating as the self-test area one or several Sub-aperture on the testing face surface error that were arbitrarily different from the sub-aperture selected by the test, and comparing the surface error of the location of the self-test sub-aperture on the stitch surface error with the self-test sub-aperture face surface error obtained from the test. In the testing experiment of a large convex

Table 2
Results of tolerance analysis for each adjustment.

Parameters		Tolerance	Wavefront Variation (λ)
Distance between CGH and the examined mirror		1.6 μm	0.0039
Tilt of CGH	X	0.7″	0.0030
	Y	0.8″	0.0024
Decentration of CGH	X	4.0 μm	0.0025
	Y	3.5 μm	0.0031
Tilt of the examined mirror	X	1.6″	0.0031
	Y	1.3″	0.0025
Decentration of the examined mirror	X	2.0 μm	0.0025
	Y	1.8 μm	0.0032
RMS			0.00794 (5.02 nm)

Table 3
Testing accuracy of the full-caliber stitching compensation.

Error	Value
Measuring random error	2.50 nm
Interferometer standard lens error	1.00 nm
CGH manufacturing error	3.67 nm
Error of each adjustment quantity	5.02 nm
Accuracy of stitching algorithm	10.12 nm
Test accuracy	12.47 nm

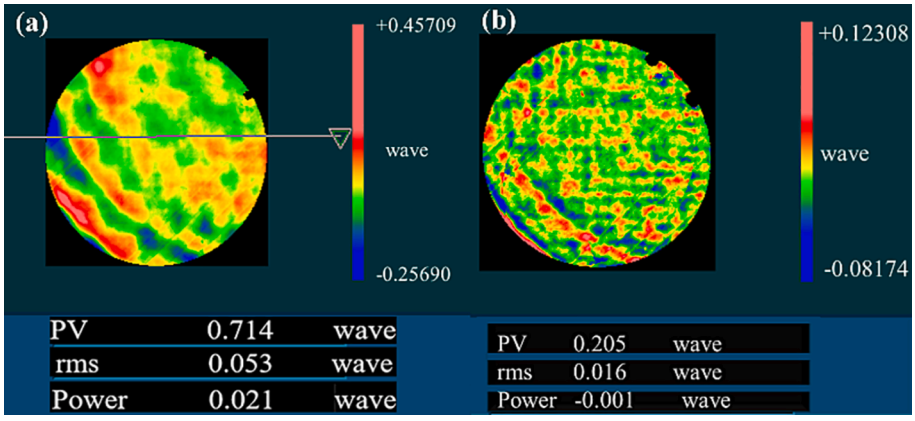

Fig. 8. (a)The result of self-testing aperture. (b)The self-test sub-aperture and residuals of the stitching results.

aspheric mirror, a position of 45° was selected as the self-checking sub-aperture. Fig. 8(a) shows the results, with the value were 0.714λ (PV) and 0.053λ(RMS). The results of the self-checked sub-aperture were point-to-point subtracted from the corresponding positions of the surface error of the stitch testin, and the residual plots are shown in Fig. 8 (b) The PV value was 0.205λ and the RMS value was 0.016λ. Thus, the feasibility of the stitching method was verified.

In the testing process, the impact of the adjustment error of the CGH on the testing results was analyzed. The adjustment error of the CGH included the distance between the CGH and the examined mirror, distance between the interferometer and the CGH, tilt of the CGH (x and y-direction tilt), eccentricity of the CGH (x and y-direction eccentricity), tilt of the examined mirror (x and y-direction tilt), and eccentricity of the examined mirror (x and y-direction eccentricity). According to the designed optical path, because the beam between the interferometer and the CGH was parallel, the distance variation between the two did not affect the testing results, and this tolerance could be neglected. Considering the processing level, the other tolerances were analyzed using design-software. When the PV value was changed by 0.25λ, the test fringe pattern changed. Table 2 presents the results of the tolerance analysis for each adjustment.

An ideal experiment is conducted in an environment with constant temperature and pressure. However, actual experimental environments have temperature and pressure variations (caused by, for example, other light sources, vibrations, noise, and airflow), and these variations can generate slight perturbations in laser wavelengths. According to previous experiments, the magnitude of the random errors in the laser wavelength during the testing process is generally 2.50 nm. Thus, we adopted this error for the experiments in this study.

Accuracy of full-diameter stitching compensation testing

The CGH-based stitching compensation method results for testing the accuracy of the full-aperture surface error of large convex aspherical mirrors is shown in Table 3. The fitting result had an RMS of 12.47 nm, which was less than λ/50, proving the feasibility of this testing method.

Conclusion

In this study, Null-Compensation testing and Non-null testing methods were combined to obtain the full-aperture surface error of large convex aspheres using sub-aperture stitching, thus achieving high-precision testing. The central and outer circle apertures were measured using the interferometer direct testing and CGH compensation methods, respectively, and a large convex aspheric surface of 538 mm was tested by combining the examples. The obtained stitching results were 1.342λ (PV) and 0.075λ (RMS). The residual of RMS was less than λ/20, which was obtained by means of two full-aperture testing methods, contour meter Luphoscan testing, and Null-Compensation testing. The stitching results were obtained via point-to-point subtraction of the residual map. The results were less than λ/50, which verifies that the proposed method can achieve high accuracy for testing large convex aspheres.

Funding

National Natural Science Foundation Instrumentation Special Project of China - High Precision Wide Dynamic Large Aperture Optical Detection System for Fine Astronomy Observation (62127901); Chinese Academy of Sciences University Student Innovation Practice Training Program (Y9I838S); Pre-research Common Technology Project for Equipment (50923020201); Key Basic Research Project of Basic Strengthening Plan (2021-JCQC-ZD-074–12-04); Basic Strengthening Plan Project (2022-JCJQ-JJ-0777).

CRediT authorship contribution statement

Xiaokun Wang: Writing – review & editing, Writing – original draft, Visualization, Validation, Supervision, Software, Resources, Project administration, Methodology, Investigation, Funding acquisition, Formal analysis, Data curation, Conceptualization. **Zhongkai Liu:** Writing – review & editing, Writing – original draft, Software, Resources, Project administration, Methodology, Investigation, Formal analysis, Data curation. **Hang Su:** Writing – original draft, Visualization, Validation, Supervision, Software, Methodology, Investigation, Funding acquisition, Data curation, Conceptualization. **Qiang Cheng:** Validation, Resources, Methodology, Investigation. **Lingzhong Li:** Software, Methodology, Investigation. **Fukun Li:** Methodology, Investigation. **Wenyan Li:** Writing – review & editing, Methodology, Formal analysis. **Bin Liu:** Investigation, Formal analysis. **Jing Wang:** Software, Investigation, Formal analysis. **Mengxue Cai:** Writing – review & editing, Investigation, Formal analysis. **Jincheng Wang:** Writing – review & editing, Investigation. **Wenhan Li:** Writing – review & editing, Methodology, Formal analysis. **Luojia Zhang:** Investigation. **Qiong Wu:** Validation, Resources, Methodology, Investigation. **Xiao Luo:** Funding acquisition. **Xuejun Zhang:** Funding acquisition.

Declaration of Competing Interest

The authors declare that they have no known competing financial interests or personal relationships that could have appeared to influence the work reported in this paper.

Data availability

Data will be made available on request.

References

[1] Xiong L, et al. Stitching swing arm profilometer test for large aperture aspher"cs. Chin Opt Lett 2019;17(11):112201.
[2] Xue S, Chen S, Guipeng T. Near-null interferometry using an aspheric null lens generating a broad range of variable spherical aberration for flexible test of aspheres. Opt Express 2018;26(24):31172–89.
[3] Utrera DG, et al. Null-screen testing of the complementary freeform surfaces of an adjustable focus lens. Opt Express 2021;29(14):21698–710.
[4] Chen S, et al. Subaperture stitching test of convex aspheres by using the reconfigurable optical null. Opt Laser Technol 2017;91:175–84.
[5] Xiaokun W, Lihui W, Zheng L. Application of subaperture stitching technology to test of large and steep aspherical surface. High Power Laser Part Beams 2007;19(7):1144.
[6] Luo X. High-precision fabrication of 4m SiC aspheric mirror. Light Sci Appl 2023;12:4.
[7] Zhang X, Hu H, Wang X, Luo X, Zhang Ge, Zhao W, et al. Challenges and strategies in high-accuracy manufacturing of the world's largest SiC aspheric mirror. Light Sci Appl 2022;11(1).
[8] Xiong J, Wu ST. Planar liquid crystal polarization optics for augmented reality and virtual reality: from fundamentals to applications. eLight 2021;1:3.
[9] Huang G, Liu Y, Wang D, Zhu Y, Wen S, Ruan J, et al. Upconversion nanoparticles for super-resolution quantification of single small extracellular vesicles. eLight 2022;2(1).
[10] Ni Y, Chen C, Wen S, Xue X, Sun L, Yang Y. Computational spectropolarimetry with a tunable liquid crystal metasurface. eLight 2022;2(1).
[11] Yan L, et al. Non-null testing for standard quadric surfaces with subaperture stitching technique. Opt Commun 2015;340:159–64.
[12] Yan F, et al. Measurement of large convex hyperbolic mirrors using hindle and stitching methods. Opt Lasers Eng 2013;51(7):856–60.
[13] Yan F, et al. Testing convex hyperbolic mirrors with two or more annuluses by Hindle and stitching methods. Opt Lasers Eng 2014;61:52–6.
[14] Fengwei L, et al. Overview of advanced manufacturing technology of large-aperture aspheric mirror. Opto-Electron Eng 2020;47(10):200203–1200201.
[15] Larsson J, et al. JWST NIRSpec observations of supernova 1987A—from the inner ejecta to the reverse sh"ck. The Astrophysical Journal Letters 2023;949(2):L27.
[16] Marini E, et al. Understanding the evolution and dust formation of carbon stars in the Large Magellanic Cloud via the J"ST. A & A 2021;647:A69.
[17] Wang Xiaokun, Qi Erhui, Hu Haixiang, et al. Optical testing of the super-large plane mirror (Invited) [J]. Infrared and Laser Engineering, 2022, 51(1): 20210953. (in Chinese); Paul Murphy, Greg Forbes, Jon Fleig, Paul Dumas, and Marc Trica"d, "Stitching Interferometry: A Flexible Solution for Surface Metrol"gy," Optics & Photonics News 14(5), 38-43 (2003).

[18] Chen W, et al. Null test of large convex aspheres by subaperture stitching with replaceable holograms. Opt Commun 2020;466:125665.
[19] Novak M, Zhao C, Burge JH. Distortion Mapping Correction in Aspheric Null Testing. In: Interferometry XIV: Techniques and Analysis; 2008. SPIE.
[20] Díaz-Uribe R, Campos-Garcia Manuel. Null-screen testing of fast convex aspheric surfaces. Appl Opt 2000;39:2670–7.
[21] Zhao C, James HB. Stitching of off-Axis Sub-Aperture Null Measurements of an Aspheric Surface. In: Interferometry XIV: Techniques and Analysis; 2008. SPIE.
[22] Liu D, et al. Non-null interferometric aspheric testing with partial null lens and reverse optimization. In: Optical Manufacturing and Testing VIII; 2009. SPIE.
[23] Elloumi M, et al. Error correction algorithms in non-null aspheric testing next generation sequencing data. Alex Eng J 2022;61(12):9819–29.
[24] Liang ZJ, et al. Advances in research and applications of optical aspheric surface metrology. Chinese Opticals 2022;15(2):161–86.
[25] Li M, et al. Modeling and suppressing the wavefront degeneration in a CGH interferometric null test. Opt Express 2022;30(23):41508–23.
[26] Baer G, Garbusi E, Lyda W, Pruss C, Osten W. Automated alignment of aspheric and freeform surfaces in a non-null test interferometer. In: Lehmann PH, Osten W, Gastinger K, editors. Presented at the SPIE Optical Metrology; 2011. 80821L. https://doi.org/10.1117/12.895010.
[27] Baer G, Schindler J, Siepmann J, Pruß C, Osten W, Schulz M. Measurement of aspheres and free-form surfaces in a non-null test interferometer: reconstruction of high-frequency errors. In: Lehmann PH, Osten W, Albertazzi A, editors. Presented at the SPIE Optical Metrology 2013, Munich, Germany; 2013. p. 878818. https://doi.org/10.1117/12.2021518.
[28] Beisswanger R, Pruss C, Schober C, Harsch A, Osten W, Lehmann P, Osten W, Albertazzi Gonçalves A. Tilted wave interferometer in common path configuration: challenges and realizationTilted wave interferometer in common path configuration: challenges and realization. In: Optical Measurement Systems for Industrial Inspection XI. Presented at the Optical Measurement Systems for Industrial Inspection XI. Munich, Germany: SPIE; 2019. p. 51. https://doi.org/10.1117/12.2526175.
[29] Garbusi E, Osten W. Perturbation methods in optics: application to the interferometric measurement of surfaces. J Opt Soc Am A 2009;26:2538. https://doi.org/10.1364/JOSAA.26.002538.
[30] Garbusi E, Pruss C, Osten W. Interferometer for precise and flexible asphere testing. Opt Lett 2008;33:2973–5. https://doi.org/10.1364/OL.33.002973.
[31] Haberl A, Pruss C, Osten W, Harsch A. Tilted wave interferometry for testing large surfaces. In: Schopf C, Rascher R, editors. Fifth European Seminar on Precision Optics Manufacturing. Presented at the Fifth European Seminar on Precision Optics Manufacturing; 2018. p. 10. https://doi.org/10.1117/12.2318573.
[32] Schober C, Beisswanger R, Gronle A, Pruss C, Osten W. Tilted Wave Fizeau Interferometer for Flexible and Robust Asphere and Freeform Testing. Light: Adv. Manuf. 2022;3:1. https://doi.org/10.37188/lam.2022.048.
[33] Chaudhuri R, Wansha A, Porras-Aguilar R, Rolland JP. Implementation of a null test for freeform optics using a high-definition spatial light modulator. Opt Express 2022;30(24):43938.
[34] Ma Xinxue, et al. The research on optical free-form metrology technologies. 10th International Symposium on Advanced Optical Manufacturing and Testing Technologies: Advanced Optical Manufacturing and Metrology Technologies. SPIE; 2021.
[35] Zhang X, et al. Wavefront optical spacing of freeform surfaces and its measurement using CGH interferometry. Opt Lasers Eng 2023;161:107350.
[36] Ye J, et al. In-situ deflectometic measurement of transparent optics in precision robotic polishing. Precis Eng 2020;64:63–9.
[37] Löh C, Moraschini M, Raptis G. On the simplicial volume and the Euler characteristic of (aspherical) manifolds. Res Math Sci 2022;9(3):44.
[38] Chen Y, et al. Transition imaging phase measuring deflectometry for high-precision measurement of optical surfaces. Measurement 2022;199:111589.
[39] Niu Z, et al. Adaptive phase correction for phase measuring deflectometry based on light field modulation. IEEE Trans Instrum Meas 2021;70:1–10.